









4–8 GHz Fourier-domain Searches for Galactic Center Pulsars

AKSHAY SURESH ^{1,2} JAMES M. CORDES ¹ SHAMI CHATTERJEE ¹ VISHAL GAJJAR ²
KAREN I. PEREZ ³ ANDREW P. V. SIEMION ^{2,4,5,6} MATT LEBOFKY ²
DAVID H. E. MACMAHON² AND CHERRY NG ^{7,2,5}

¹*Cornell Center for Astrophysics and Planetary Science, and Department of Astronomy, Cornell University, Ithaca, NY 14853, USA*

²*Breakthrough Listen, University of California, Berkeley, CA 94720, USA*

³*Department of Astronomy, Columbia University, 550 West 120th Street, New York, NY 10027, USA*

⁴*Department of Astrophysics/IMAPP, Radboud University, Nijmegen, The Netherlands*

⁵*SETI Institute, Mountain View, CA 94043, USA*

⁶*University of Malta, Institute of Space Sciences and Astronomy, Malta*

⁷*Dunlap Institute for Astronomy & Astrophysics, University of Toronto, 50 St. George Street, Toronto, ON M5S 3H4, Canada*

ABSTRACT

The Galactic Center (GC), with its high density of massive stars, is a promising target for radio transient searches. In particular, the discovery and timing of a pulsar orbiting the central supermassive black hole (SMBH) of our Galaxy will enable stringent strong-field tests of gravity and accurate measurements of SMBH properties. We performed multi-epoch 4–8 GHz observations of the inner ≈ 15 pc of our Galaxy using the Robert C. Byrd Green Bank Telescope in 2019 August–September. Our investigations constitute the most sensitive 4–8 GHz GC pulsar survey conducted to date, reaching down to a 6.1 GHz pseudo-luminosity threshold of ≈ 1 mJy kpc² for a pulse duty cycle of 2.5%. We searched our data in the Fourier-domain for periodic signals incorporating a constant or linearly changing line-of-sight pulsar acceleration. We report the successful detection of the GC magnetar PSR J1745–2900 in our data. Our pulsar searches yielded a non-detection of novel periodic astrophysical emissions above a 6σ detection threshold in harmonic-summed power spectra. We reconcile our non-detection of GC pulsars with inadequate sensitivity to a likely GC pulsar population dominated by millisecond pulsars. Alternatively, close encounters with compact objects in the dense GC environment may scatter pulsars away from the GC. The dense central interstellar medium may also favorably produce magnetars over pulsars.

Keywords: Galactic Center (565) — Neutron stars (1108) — Radio pulsars (1353) — Radio transient sources (2008)

1. INTRODUCTION

The central parsec of our Galaxy hosts a dense nuclear star cluster (NSC, Schödel

et al. 2007) surrounding the supermassive black hole (SMBH), Sgr A* of mass $M_{\text{SgrA}^*} \approx (4.30 \pm 0.01) \times 10^6 M_{\odot}$ (GRAVITY Collaboration et al. 2021). The Galactic NSC, while primarily containing old, late-type stars (≥ 10 Gyr, Schödel et al. 2020), is home to a large population of neutron star and black hole (BH) progenitors, including young, massive main-sequence stars (Ghez et al. 2005; Genzel et al. 2010) and Wolf-Rayet stars (Pau-mard et al. 2001). Recent detections of numerous X-ray binaries (Hailey et al. 2018; Zhu et al. 2018) and compact steep-spectrum radio sources (Chiti et al. 2016; Hyman et al. 2005, 2009, 2021; Zhao et al. 2020, 2022) further indicate a likely abundance of neutron stars and stellar-mass BHs in the NSC. Considering multiwavelength constraints on the known neutron star population, Wharton et al. (2012) argued for the existence of $\sim 10^3$ radio pulsars actively beaming towards the Earth from the inner parsec of our Galaxy. Several of these pulsars may potentially reside in binaries, analogous to the profusion of millisecond pulsars¹ (MSPs) seen in globular clusters (Ransom 2008). Additionally, a substantial MSP population (Brandt & Kocsis 2015; Lee et al. 2015; Bartels et al. 2016; Fragione et al. 2018) in the NSC has been postulated as a plausible explanation for the observed diffuse γ -ray excess around Sgr A* (Ackermann et al. 2014; Ajello et al. 2016); another being dark matter annihilation (Abazajian et al. 2014; Calore et al. 2015) at the Galactic Center (GC).

Enabling powerful strong-field tests of gravity (Wex & Kopeikin 1999; Kramer et al. 2004; Liu et al. 2012; Wex 2014; Psaltis et al. 2016), the discovery and timing of even a canonical pulsar² (CP) in a binary with a BH will allow

rigorous tests of the Cosmic Censorship Conjecture (Penrose 1969, 1999) and the BH No Hair theorem. Furthermore, if orbiting close enough (binary orbital period, $P_b \lesssim 1$ yr) to Sgr A*, regular pulsar timing efforts will permit accurate measurements of SMBH mass (anticipated precision $\simeq 1$ – $10 M_{\odot}$ with weekly observing cadence over five years, Liu et al. 2012), spin, and quadrupole moment. Finally, radio observations of pulse dispersion, scattering, and Faraday rotation will provide unique probes of the turbulent, magneto-ionic central interstellar medium (ISM) of our Galaxy.

Motivated by the rich rewards of GC pulsar timing, numerous extensive surveys of the GC have been previously undertaken over a broad range of radio frequencies (e.g., Johnston et al. 2006; Deneva et al. 2009; Macquart et al. 2010; Bates et al. 2011; Siemion et al. 2013; Eatough et al. 2013a,b, 2021; Liu et al. 2021; Torne et al. 2021, etc.). To date, these endeavors have revealed a single magnetar, namely PSR J1745–2900 (Eatough et al. 2013b) at $2''.4$ offset from Sgr A*, and five pulsars, all located $\gtrsim 10'$ away from Sgr A*. The hitherto non-detection of pulsars within a $10'$ radius of Sgr A*, termed the “missing pulsar problem,” is often attributed to hyperstrong interstellar scattering in the direction of the GC (Cordes & Lazio 1997; Lazio & Cordes 1998a,b; Cordes & Lazio 2002). While pulse broadening measurements of PSR J1745–2900 suggest otherwise (Spitler et al. 2014), it is unclear if a single line of sight towards the GC magnetar is representative of a possibly complex scattering structure at the GC (Cordes & Lazio 2002; Schnitzeler et al. 2016; Dexter et al. 2017). Alternatively, an abundance of highly magnetized massive stars in the NSC may preferentially produce magnetars over spin-driven pulsars (Dexter & O’Leary 2014).

¹ We define MSPs as pulsars with barycentric rotational periods, $P_0 < 30$ ms.

² We define CPs as pulsars with $P_0 \geq 30$ ms.

Aside from scattering, additional obstacles to GC pulsar discovery include the Galactic background temperature ($T_{\text{GC}}(\nu)$: Law et al. 2008), free-free absorption by the ionized central ISM, and orbital motion (if in multi-object systems). While observations at high radio frequencies ($\nu \gtrsim 10$ GHz) help mitigate $T_{\text{GC}}(\nu)$ and free-free absorption, pulsar emission also significantly weakens with increasing ν (period-averaged flux density, $S_\nu \propto \nu^{-1.4 \pm 1.0}$, Bates et al. 2013). Weighing various chromatic challenges to GC pulsar discovery, Rajwade et al. (2017) recommended 9–13 GHz as the optimal observing band for GC pulsar surveys. However, the observed broad spread of pulsar spectral indices (Bates et al. 2013) mandates continued broadband monitoring to detect elusive GC pulsars.

Orbital motion limits pulsar detection by smearing harmonics of the pulsar rotational frequency ($f_0 = 1/P_0$) in the power spectrum. Standard Fourier-domain algorithms attempt to correct for this smearing assuming either a constant or linearly changing radial pulsar acceleration. Such implementations work for integration times, $T \lesssim 0.10P_b$ and $T \lesssim 0.15P_b$, respectively (Ransom et al. 2002; Andersen & Ransom 2018). While acceleration and jerk searches favor shorter T to counter orbital motion, the sensitivity to a single harmonic in the power spectrum also drops with decreasing T . Integration times in Fourier-domain pulsar searches must therefore strike a delicate balance between maximizing the single harmonic sensitivity and mitigating power smearing from orbital motion.

Here, we leverage $T \in \{5, 30, 60\}$ minutes in the 4–8 GHz Breakthrough Listen (BL) GC survey (Gajjar et al. 2021) to conduct sensitive searches for pulsars orbiting Sgr A* or stellar-mass BHs. Section 2 describes our observations

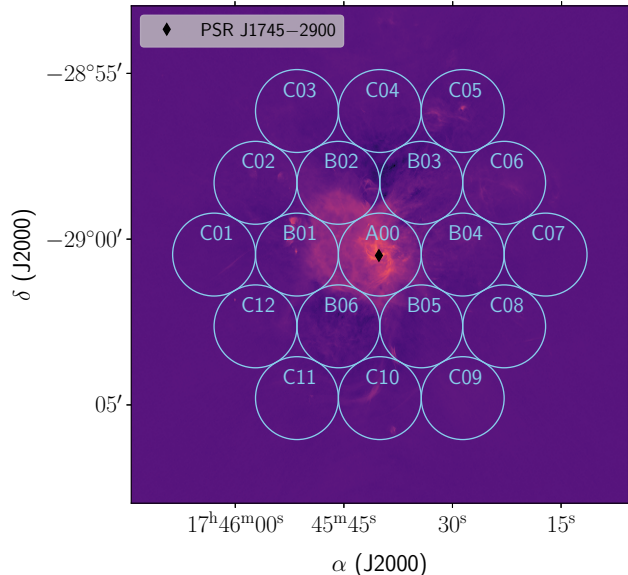


Figure 1. 4–8 GHz BL GC survey field comprised of 19 distinct pointings (light blue circles) of $\theta_{\text{HPBW}} \approx 2.5'$ each. The background image is a 5.5 GHz Jansky Very Large Array continuum image (Zhao et al. 2016) of the Sgr A* complex. The GC magnetar PSR J1745–2900 (black diamond) is contained in our central pointing A00. All known pulsars lie $\gtrsim 10'$ away from Sgr A*, i.e., outside of our survey footprint.

and data preprocessing. In Section 3, we present our pulsar search methodology and results. We estimate our survey sensitivity to periodic signals in Section 4. Ultimately, we summarize our key findings and discuss their physical significance in Section 5.

2. OBSERVATIONS

The BL GC survey is an extensive 0.7–93 GHz search of the GC and neighboring Galactic bulge fields for radio technosignatures, pulsars, bursts, spectral lines, and masers (see Gajjar et al. 2021 for the full survey description, data products, and early technosignature and burst science results). The 4–93 GHz component of the survey utilizes the Robert C. Byrd Green Bank Telescope (GBT), whereas the 0.7–4 GHz portion uses the Parkes radio telescope. Figure 1 shows the 4–8 GHz survey field, wherein a

Table 1. Log of 4–8 GHz GBT observations analyzed in our study.

| Epoch (number) | Start date (UTC) | Start MJD (UTC) | Test pulsars | Pointings | N_{scans}^a | Scan duration (minutes) |
|-------------------|---------------------|--------------------|----------------------|------------|----------------------|----------------------------|
| 1 | 2019 Aug 7 | 58702.217 | B0355+54, J1744–1134 | (C01, C07) | (3, 2) | 5 |
| 2 | 2019 Aug 9 | 58704.993 | B1133+16, J1744–1134 | C07 | 1 | 5 |
| | | | | (B01, B04) | (3, 3) | 5 |
| | | | | (B02, B05) | (3, 3) | 5 |
| | | | | (B03, B06) | (3, 3) | 5 |
| | | | | (C02, C04) | (3, 3) | 5 |
| | | | | (C03, C05) | (3, 3) | 5 |
| | | | | (C06, C08) | (3, 3) | 5 |
| | | | | (C09, C11) | (3, 3) | 5 |
| | | | | (C10, C12) | (2, 3) | 5 |
| | | | | A00 | 1 | 60 |
| 3 | 2019 Sep 8 | 58734.958 | ... | A00 | 2 | 30 |
| 4 ^b | 2019 Sep 11 | 58737.962 | B2021+51 | A00 | 8 | 30 |

^aNo. of scans per pointing. For a pointing pair (X, Y), (N_X, N_Y) denotes the no. of scans of X and Y respectively.

^bEpoch 4 included position-switched observations of the flux density calibrator 3C 286.

NOTE—Data available for download at the following links.

<http://blpd9.ssl.berkeley.edu/GCrawspec>

<http://blpd12.ssl.berkeley.edu/GCrawspec>

6′25 radius of the GC is covered by 19 distinct GBT pointings arranged in three concentric hexagonal rings. From inner to outer, these rings are labeled A, B, and C, with 1, 6, and 12 pointings per ring respectively. All pointings used the single-beam C-band receiver, yielding a half-power beam width, $\theta_{\text{HPBW}} \approx 2'.5$ at 6 GHz. As illustrated in Figure 1, our central pointing A00 contains the GC magnetar. We refer readers to Suresh et al. (2021) for a 4–8 GHz study of the GC magnetar using our A00 data.

Table 1 presents an overview of our 4–8 GHz observations distributed across four epochs during 2019 August–September. Our observing program consists of eleven deep integrations (≥ 30 minutes) on A00, two 5-minute scans on C10, and three 5-minute cadences on each

of the remaining pointings. In addition, we observed test pulsars at three epochs, and confirmed their respective detections to verify our system integrity. To identify and reject radio frequency interference (RFI) via position switching, we conducted alternating observations of pairs of pointings in rings B and C. Pointing pairs were chosen such that the beam centers of grouped pointings were separated by at least $2\theta_{\text{HPBW}}$ on the sky.

To accommodate various science cases, baseband voltages gathered during our observations were channelized to different spectral and temporal resolutions using the Breakthrough Listen Digital Backend (MacMahon et al. 2018; Lebofsky et al. 2019). Here, for our pulsar searches, we worked with total intensity filterbank data (no coherent dedispersion performed) having

$\approx 43.69 \mu\text{s}$ time sampling and $\approx 91.67 \text{ kHz}$ channel bandwidth. These data contain 53,248 channels spanning 3.56–8.44 GHz, which covers the 3.9–8.0 GHz instantaneous response of the C-band receiver.

2.1. Data preprocessing

We followed the methodology of Suresh et al. (2021) to excise RFI from our data using the `rfifind` module of the pulsar software package PRESTO (Ransom 2011). Adopting an integration time of 1 s for our `rfifind` runs, we detected bright, persistent interference between 4.24–4.39, 4.90–4.95, and 6.90–7.10 GHz. Incorporating our `rfifind` mask and clipping bandpass edges, the usable radio frequency band in our data extends between 4.4–8.0 GHz.

After RFI masking, we dedispersed our dynamic spectra (radio frequency-time data) at 1836 trial DMs between 0 pc cm^{-3} and 5505 pc cm^{-3} (both limits included) with a grid spacing of 3 pc cm^{-3} . These dedispersed data were summed over the entire usable band, and then block-averaged by a factor of 8 to output dedispersed time series with a sample interval, $t_{\text{samp}} \approx 349.53 \mu\text{s}$.

2.2. Red noise removal

Slow pulsar discovery ($P_0 \geq 1 \text{ s}$) in long time series ($T \geq 5 \text{ minutes}$) often suffers from the presence of low-frequency noise in Fourier-domain spectra. To alleviate the adverse impact of red noise on our pulsar searches, we detrended our dedispersed time series using a running median window of width W_{med} .

For deciding an optimal value of W_{med} , we visually inspected the effect of different trial W_{med} on power spectra of barycentric GC magnetar time series (DM = 1776 pc cm^{-3} , $f_0^{\text{mag}} = 1/P_0^{\text{mag}} \approx 0.2653 \text{ Hz}$, Suresh et al. 2021). Starting at $W_{\text{med}} = 4 \text{ s}$, we successively lowered W_{med} by factors of 2 until further reduction in W_{med}

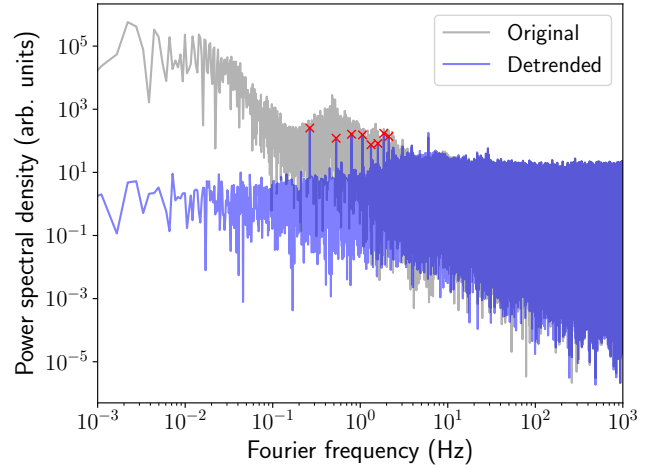


Figure 2. Power spectra of barycentric DM = 1776 pc cm^{-3} time series from a 30-minutes A00 scan before (gray) and after (blue) detrending with a running median filter of width 0.25 s. The red crosses label the fundamental rotation frequency of the GC magnetar and its harmonics. The red noise in the gray power spectrum below 4 Hz arises from gradual baseline fluctuations in our original time series.

brought no concomitant increase in the number of harmonics of f_0^{mag} seen in the power spectrum. In doing so, we settled at $W_{\text{med}} = 0.25 \text{ s}$ for removing slow baseline fluctuations in our dedispersed time series.

Figure 2 shows the result of time series detrending on the power spectrum of a barycentric DM = 1776 pc cm^{-3} time series from a 30-minutes A00 scan. The power spectrum of the detrended time series evidently reveals significant peaks at f_0^{mag} and its first seven harmonics. Without detrending, these peaks remain buried within red noise in the power spectrum of the original time series.

Finally, to limit the false positive count in our pulsar searches, we masked periodic RFI in the power spectra of our detrended time series. Looking at power spectra of topocentric DM = 0 pc cm^{-3} time series, we identified and flagged significant spikes at frequencies of 1.2,

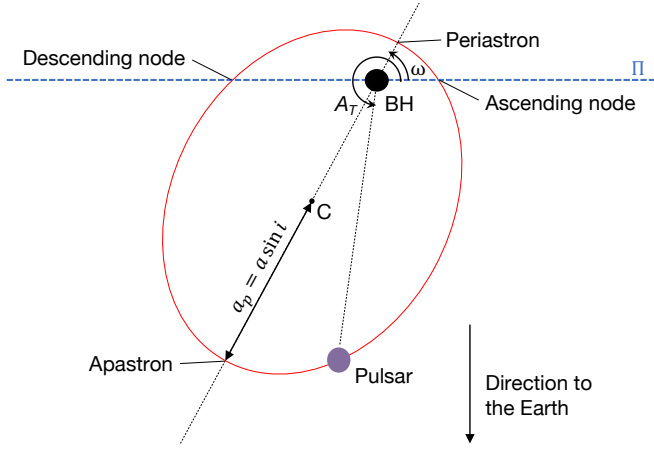


Figure 3. A pulsar orbiting a black hole. The pulsar orbit (red ellipse) has been projected onto a plane containing the direction to the Earth and the line Π connecting the two nodes. The symbols a , i , ω , and A_T represent, respectively, the orbital semi-major axis, the orbital inclination, the argument of periapsis, and the pulsar true anomaly. The quantity $a_p = a \sin i$ is the projected semi-major axis of the pulsar orbit centered at C .

6, 60 Hz (US electric power line frequency), and their first five harmonics. The resulting cleaned power spectra constituted the basis of our Fourier-domain periodicity searches.

3. PERIODICITY SEARCHES

Consider a regular pulse train (insignificant pulse jitter) from an isolated pulsar of barycentric rotational frequency, $f_0 = 1/P_0$. For an effective pulse duty cycle δ_{eff} , the energy in the pulse train gets distributed over $N_h \simeq 1/2\delta_{\text{eff}}$ independent harmonics in the power spectrum. Consequently, standard periodicity searches perform harmonic summing in power spectra of dedispersed time series to increase the significance of a pulsar detection (Ransom et al. 2002). In a blind search, the pulsar DM, f_0 , and δ_{eff} are unknown a priori. Searches for isolated pulsars, hence require sampling of the three-dimensional parameter space $\text{DM}-f-N_h$.

Binary orbital motion complicates pulsar detection by introducing a time-dependent

Doppler drift that smears harmonics in the power spectrum. Conventional search algorithms attempt to retroactively correct for this smearing by presuming a constant or linearly evolving line-of-sight pulsar acceleration (Ransom et al. 2002; Andersen & Ransom 2018).

Figure 3 shows a binary pulsar orbit and its Keplerian orbital elements, including its projected semi-major axis $a_p = a \sin i$ (orbital semi-major axis a and inclination i), argument of periapsis ω , and true anomaly A_T . In the Newtonian regime, the line-of-sight pulsar acceleration (a_l) and jerk (j_l) are respectively given by (Bagchi et al. 2013; Liu et al. 2021)

$$a_l = - \left(\frac{2\pi}{P_b} \right)^2 \frac{a_p}{(1-e^2)^2} (1 + e \cos A_T)^2 \times \sin(A_T + \omega), \quad (1)$$

$$j_l = - \left(\frac{2\pi}{P_b} \right)^3 \frac{a_p}{(1-e^2)^{7/2}} (1 + e \cos A_T)^3 [e \cos \omega + \cos(A_T + \omega) - 3e \sin(A_T + \omega) \sin A_T]. \quad (2)$$

In the above equations, e denotes the eccentricity of the pulsar orbit. Casting a_l and j_l in dimensionless units, and introducing the harmonic number h , we have

$$z = h \left(\frac{a_l f T^2}{c} \right), \quad (3)$$

$$w = h \left(\frac{j_l f T^3}{c} \right). \quad (4)$$

Here, $h = 1$ labels the fundamental frequency f , and c is the vacuum speed of light. Following Andersen & Ransom (2018), we define the dimensionless Fourier frequency, $r = fT$. The quantities z and w thus represent the number of bins of signal drift in r and \dot{r} over time T . In Equations 3 and 4, we note that both z and w

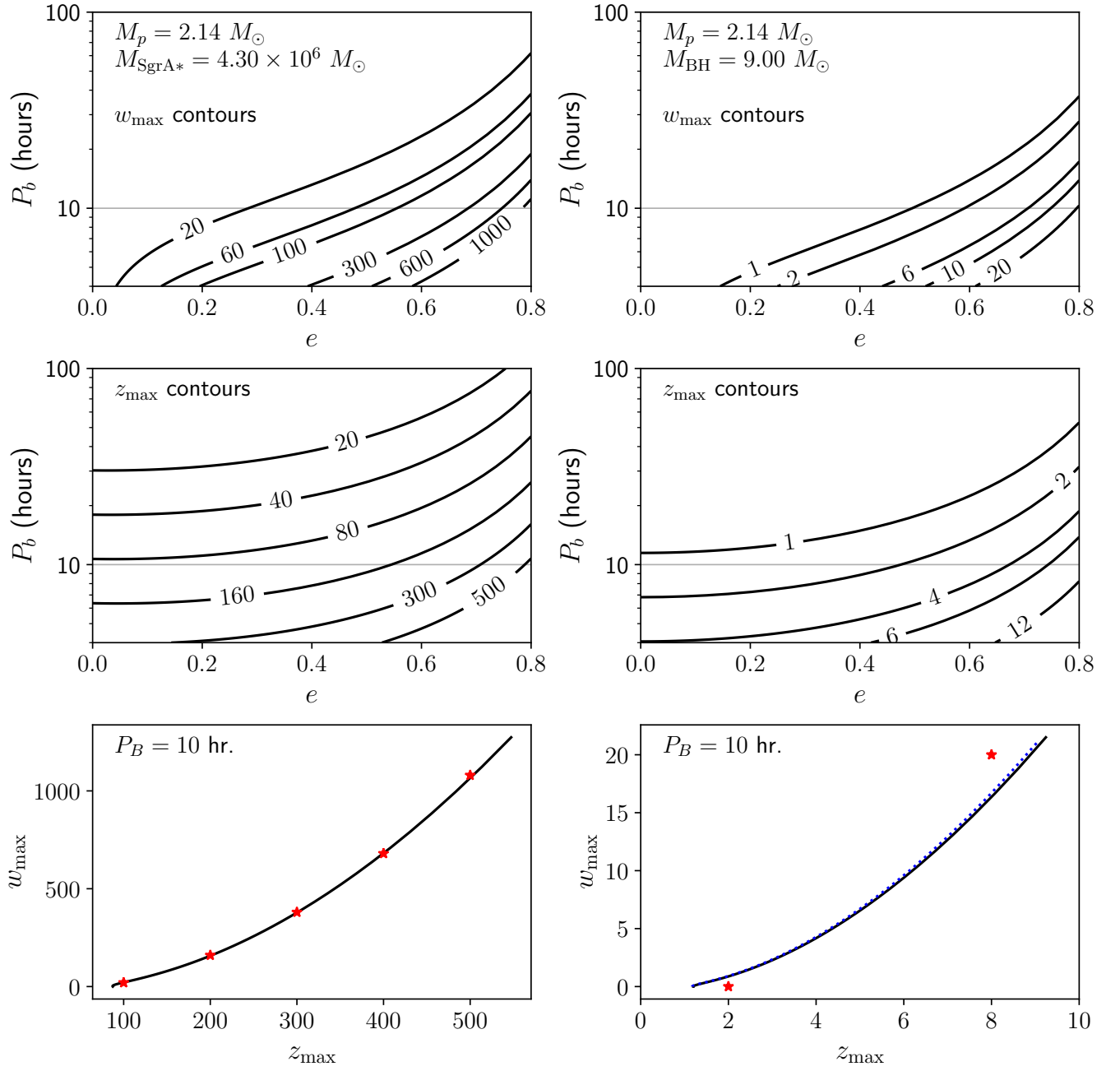


Figure 4. (z_{\max}, w_{\max}) curves for $N_h = 1$ binary pulsar searches. Top row: Contours of constant w_{\max} for a $2.14 M_{\odot}$ pulsar orbiting Sgr A* (left column) and a $9 M_{\odot}$ BH (right column). Middle row: z_{\max} contours for the same systems. Bottom row: w_{\max} vs. z_{\max} (black solid curves) for a binary orbital period of 10 hours, assuming a pulsar mass of $2.14 M_{\odot}$. While the black solid curve in the bottom left panel is insensitive to M_p , the blue dotted curve in the bottom right panel shows the corresponding trend for a $1.4 M_{\odot}$ pulsar orbiting a $9 M_{\odot}$ BH. The red stars mark (z_{\max}, w_{\max}) tuples chosen for our Fourier-domain jerk searches on $T = 30$ min. integrations. We note that the `accelsearch` module of PRESTO quantizes z_{\max} and w_{\max} in multiples of 2 and 20 respectively (Andersen & Ransom 2018). All panels assume $P_0 = 1$ s, and edge-on pulsar orbits with $\omega = 0^\circ$ and $A_T = -90^\circ$.

scale linearly with h . Therefore, orbital motion

lowers the detection significance of all harmon-

Table 2. Pulsar search parameters

| Science targets | Pointings | T^\dagger (minutes) | P_b^\ddagger (hours) | (z_{\max}, w_{\max}) |
|-----------------------------------|----------------|--------------------------|---------------------------|--|
| Isolated pulsars | All | 5, 30, 60 | ... | (0, 0) |
| Pulsars orbiting stellar-mass BHs | B-ring, C-ring | 5 | 1 | (2, 0), (6, 20) |
| | A00 | 30 | 10 | (2, 0), (8, 20) |
| Pulsars around Sgr A* | A00 | 30 | 10 | (100, 20), (200, 160), (300, 380), (400, 680), (500, 1080) |

[†]Integration time

[‡]Target binary orbital period assumed for specified (z_{\max}, w_{\max}) tuples

NOTE—

- 1836 trial DMs explored between 0–5505 pc cm⁻³ (both limits included) with a grid spacing of 3 pc cm⁻³.
- For a sample interval of $\approx 349.53 \mu\text{s}$ in the dedispersed time series, the range of f searched is 0–1430 Hz with a resolution of $1/T$.
- Trial N_h values considered = {1, 2, 4, 8}.

ics in the power spectrum, with greater deleterious effects for higher harmonics. The most minimal regime of pulsar detection then occurs when only the fundamental survives with adequate significance in the power spectrum, while all higher harmonics have been smeared into the continuum by orbital motion.

3.1. Acceleration and jerk searches

The `accelsearch` routine of PRESTO (Ransom 2011) executes a matched filtering scheme that accounts for Fourier-domain power smearing of the highest harmonic up to a Fourier acceleration z_{\max} and a Fourier jerk w_{\max} (Ransom et al. 2002; Andersen & Ransom 2018). Searches for binary pulsars, hence involve sampling over five parameters, i.e., the DM, f , N_h , z_{\max} , and w_{\max} .

We targeted the discovery of pulsars in compact orbits around Sgr A* or stellar-mass BHs. We focused our searches on CPs as we expected most MSPs to fall below our detection threshold (see Section 4). To identify suitable trial parameter values for our binary pulsar searches,

we considered a $M_p = 2.14 M_\odot$ pulsar (highest neutron star mass measured to date, Cromartie et al. 2020) located at $A_T = -90^\circ$ in an edge-on orbit ($i = 90^\circ$) with $\omega = 0^\circ$. We further envisaged $N_h = 1$ searches for pulsars in tight binaries with large a_l and j_l .

Assuming $T = 30$ minutes and $P_0 = 1$ s, Figure 4 shows contours of constant w_{\max} (top row) and z_{\max} (middle row) for pulsar orbits around Sgr A* (left column) and a $M_{\text{BH}} = 9 M_\odot$ BH (median BH mass for solar metallicity, Woosley et al. 2020). The condition $T \lesssim 0.15P_b$ for jerk searches restricts us to $P_b \gtrsim 3.3$ hours for $T = 30$ minutes. Setting $P_b = 10$ hours as our target, we sought to cover $e \in [0.0, 0.8]$ by uniformly sampling the w_{\max} vs. z_{\max} curves shown in the bottom row of Figure 4. For our selected M_{BH} value, a_p varies inappreciably for known ranges of M_p . Therefore, our chosen (z_{\max}, w_{\max}) tuples encompass all known pulsar masses, including the typical mass of $1.4 M_\odot$.

Table 3. Periodicity detection statistics

| Pointing | N_{detected}^a | N_{rejected}^b | N_{cands}^c |
|----------|-------------------------|-------------------------|----------------------|
| A00 | 7039 | ... | 7039 |
| B01 | 454 | 27 | 427 |
| B02 | 487 | 22 | 465 |
| B03 | 495 | 26 | 469 |
| B04 | 460 | 34 | 426 |
| B05 | 414 | 25 | 389 |
| B06 | 485 | 25 | 460 |
| C01 | 481 | 13 | 468 |
| C02 | 456 | 27 | 429 |
| C03 | 489 | 36 | 453 |
| C04 | 437 | 25 | 412 |
| C05 | 554 | 28 | 526 |
| C06 | 596 | 48 | 548 |
| C07 | 458 | 12 | 446 |
| C08 | 423 | 33 | 390 |
| C09 | 555 | 46 | 509 |
| C10 | 370 | 12 | 358 |
| C11 | 413 | 38 | 375 |
| C12 | 982 | 11 | 971 |
| Total | 16048 | 488 | 15560 |

^aNo. of distinct candidates detected at or above $6\sigma_{\text{ps}}$ equivalent Gaussian significance in χ^2 -distributed power spectra.

^bNo. of candidates rejected via position switching.

^cNo. of candidates that pass comparisons between periodicity detections in paired pointings.

(Zhang et al. 2011).

Table 2 outlines our pulsar search strategy, wherein we also incorporated searches for isolated pulsars and binary pulsar orbits in the $T = 5$ minutes integrations of our B- and C-ring pointings. Again, we identified viable z_{max} and w_{max} values considering $N_h = 1$ searches for binary pulsar orbits. Adopting the same $(z_{\text{max}}, w_{\text{max}})$ tuples for our $N_h = \{2, 4, 8\}$ searches, we enhance our sensitivity to slowly

orbiting pulsars through harmonic summing. However, since our searches perform matched filtering (Andersen & Ransom 2018) in the Fourier-domain, greatest sensitivity will be had for systems with $a_l = (z_{\text{max}}c/N_h f T^2)$ and $j_l = (w_{\text{max}}c/N_h f T^3)$.

Our pulsar search procedure on data can be described in three independent stages. Firstly, we ran non-accelerated searches for isolated pulsars on a per-scan basis. Secondly, at the trial parameter values listed in Table 2, we conducted acceleration and jerk searches on data from our 5-minutes and 30-minutes scans. Finally, we split our 60-minutes A00 scan from epoch 2 into two contiguous halves, and executed jerk searches separately on each half.

Imposing a $6\sigma_{\text{ps}}$ detection probability threshold in harmonic-summed power spectra, we used the `accel_sift.py` script of PRESTO (Ransom 2011) to group hits across adjacent trial DMs and frequencies f into distinct candidates. Here, σ_{ps} measures the equivalent Gaussian significance of a frequency f in the χ^2 -distributed power spectrum (assuming Gaussian white noise background in detrended time series).

3.2. Results

Our pulsar searches yielded a total of 16,048 periodicity candidates across 64 scans. Table 3 presents our candidate detection statistics organized by pointings. Since we expect any astrophysical signal of our interest to be localized on the sky, we pruned our detection list by rejecting candidates common to paired pointings within a frequency tolerance Δf and a DM tolerance ΔDM . For an integration time T , we chose $\Delta f = 1/2T$, i.e., the maximum error on f for $N_h = 1$. Given an effective pulse width $W_{\text{eff}} = \delta_{\text{eff}}P$, the DM uncertainty associated with pulse detection across a usable bandwidth

B is (Cordes & McLaughlin 2003)

$$\Delta\text{DM} \simeq 506 \text{ pc cm}^{-3} \left(\frac{W_{\text{eff,ms}} \nu_c^3}{B_{\text{MHz}}} \right). \quad (5)$$

Here, $B \approx 3.35$ GHz, and $\nu_c \approx 6.1$ GHz is the center frequency of our observations. Conservatively setting $W_{\text{eff}} = 3t_{\text{samp}} \approx 1$ ms, we obtain $\Delta\text{DM} \approx 33 \text{ pc cm}^{-3}$. As evident from Table 3, our position-switched observations permit us to eliminate about 5% of candidates in rings B and C, thereby leaving us with 15,560 periodicity detections across 64 scans.

In Figures 5 and 6, we statistically analyze the remaining 15,560 candidates in terms of their DM, period ($P = 1/f$), and σ_{ps} distributions. The GC magnetar markedly stands out as a high significance cluster of A00 candidates centered at DM = 1776 pc cm⁻³ and $P = 3.7686$ s. Furthermore, nearly 90% of candidates fall within a horizontal expanse between $P = 2$ ms and $P = 100$ ms in the P -DM plane. We attribute this scatter of candidates partly to a statistical sampling effect (greater number of power spectrum samples across $P \in [2, 100]$ ms than that spanning $P \in [10^2, 10^4]$ ms), and partly to noise and intermittent band-limited periodic RFI in dynamic spectra. Appendix A shows average profiles of two sample candidates, whose phase-resolved dynamic spectra reveal bright RFI between 4.4–4.9, 5.1–5.2, 6.8–7.0, and 7.5–7.8 GHz. These narrowband structures asynchronously wax and wane during our observations, leading to a horde of non-astrophysical candidates detected at numerous DMs and periods.

Other notable features in Figure 5 include streaks of A00 candidates at $P \in [30, 100]$ ms, and an excess of C-ring candidates at $P \lesssim 2$ ms and DM $\in [0, 150] \cup [430, 700] \cup [1000, 1150] \text{ pc cm}^{-3}$. Upon manual visual inspection of their respective folded profiles, we

traced the A00 streaks to periodic irregularities occurring near the start and end of individual scans. Further, we associate the surfeit of C-ring candidates with the emergence of bright RFI at 5.8–5.9 and 7.8–7.9 GHz during our C12 scans.

In summary, we report the successful detection of the GC magnetar in periodicity searches of our A00 scans. Setting a $6\sigma_{\text{ps}}$ detection threshold for our Fourier-domain searches, we find no statistical evidence of novel periodic astrophysical emissions in the 4–8 GHz BL GC survey data.

4. SURVEY SENSITIVITY ESTIMATION

Consider the minimal detection of a pulsar, with only its $h = 1$ harmonic visible in the power spectrum. In such a circumstance, the relevant theoretical detection limit is the single harmonic sensitivity at f_0 given by

$$S_{\text{sh}} = m \frac{S_{\text{sys}}}{\sqrt{2BT}}. \quad (6)$$

Here, S_{sys} is the system-equivalent flux density (SEFD), and $m = 6$ is the minimum significance required to claim a detection. Often, S_{sys} in GC surveys is written as a sum of two terms.

$$S_{\text{sys}}(\nu) = S_{\text{sys}}^{\text{off-SgrA}^*}(\nu) + S_{\text{sys}}^{\text{SgrA}^*}(\nu), \quad (7)$$

where $S_{\text{sys}}^{\text{off-SgrA}^*}$ is the SEFD away from the Sgr A* complex, and $S_{\text{sys}}^{\text{SgrA}^*}$ captures the SEFD contribution from the Sgr A* complex.

Assuming slow pulsar orbital motion in time T , we can lower our sensitivity threshold below S_{sh} by summing over harmonics in the power spectrum. For $\delta_{\text{eff}} \ll 1$, the corresponding minimum detectable flux density (Dewey et al. 1985) is then

$$S_{\text{min}} = m \frac{S_{\text{sys}}}{\sqrt{2BT}} \left(\frac{\delta_{\text{eff}}}{1 - \delta_{\text{eff}}} \right)^{1/2}. \quad (8)$$

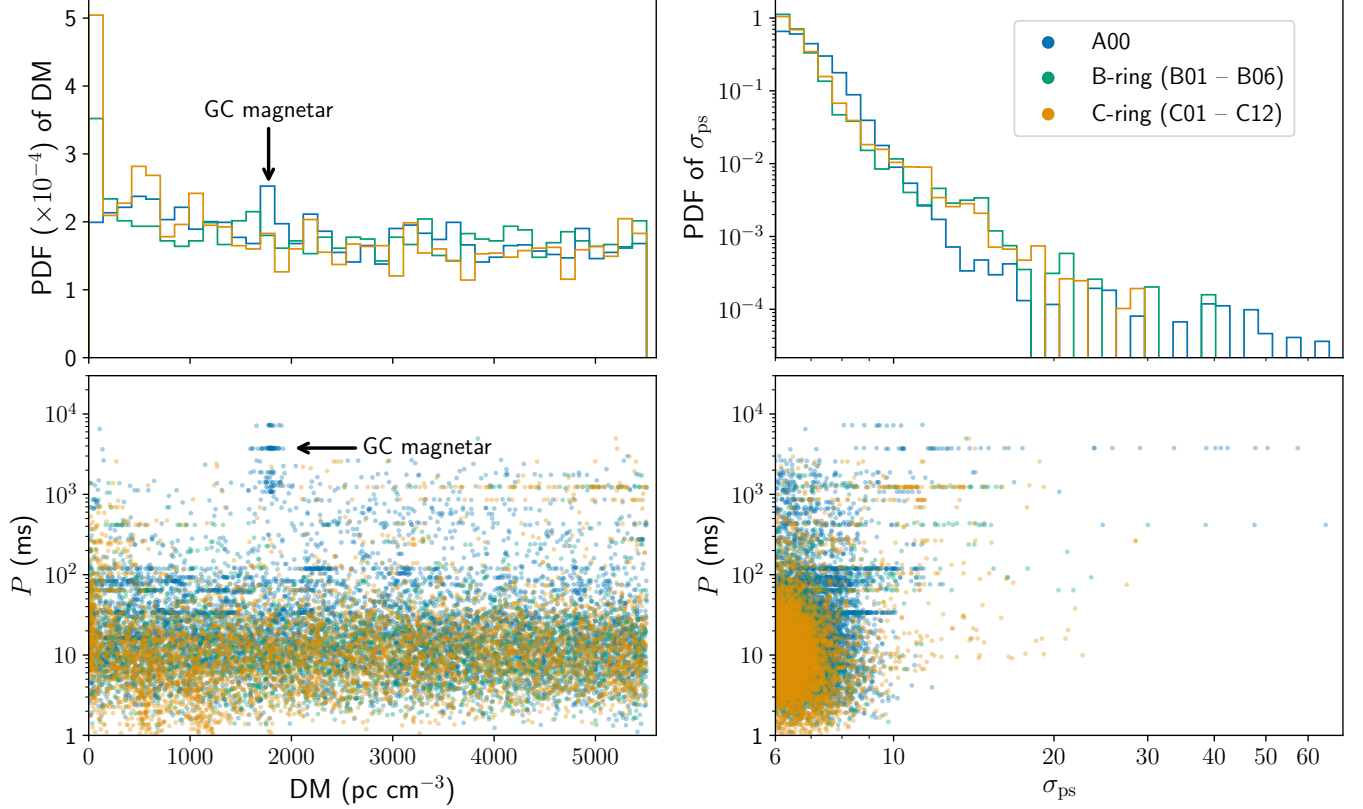


Figure 5. Top left panel: Probability distribution function (PDF) of candidate DMs binned uniformly to 141 pc cm^{-3} resolution. Top right panel: PDF of equivalent Gaussian significance (σ_{ps}) of candidates in power spectra. Plotted bins are linear in $\ln \sigma_{\text{ps}}$ with width ≈ 0.06 . Bottom left panel: Scatter of candidates in the period–DM plane. Bottom right panel: Period– σ_{ps} scatter of candidates. In all panels, the blue, green, and orange colors represent A00, B-ring, and C-ring respectively.

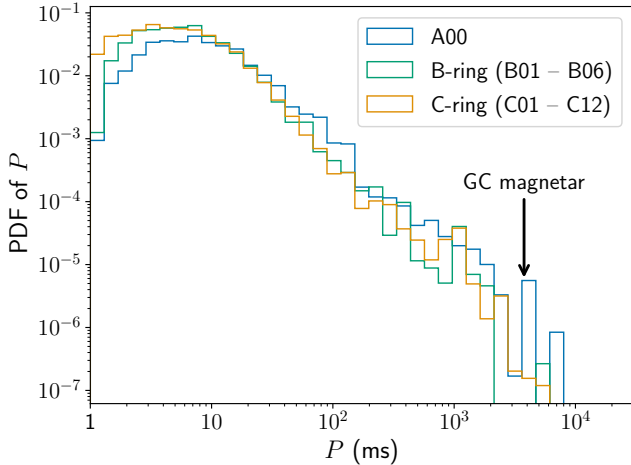


Figure 6. PDF of candidate periods (P) organized by rings. Histogram bins are evenly spaced in $\ln P$ with width $\approx 0.26 \text{ s}$.

Appendix B describes various sources of pulse broadening that can widen a pulse from intrinsic width W_{int} to effective width, $W_{\text{eff}} = \delta_{\text{eff}} P$ in a dedispersed time series. We define $\delta_{\text{int}} = W_{\text{int}}/P$ as the intrinsic pulse duty cycle. From the ATNF pulsar catalog v1.66 (Manchester et al. 2001)³, about 83% of CPs have duty cycles between 1% and 10%, with a median duty cycle of 2.5%.

Assuming negligible instrumental and dispersive pulse broadening,

$$W_{\text{eff}}(\nu) \approx (W_{\text{int}}^2 + t_{\text{samp}}^2 + \tau_{\text{sc}}^2(\nu))^{1/2}. \quad (9)$$

³ <https://www.atnf.csiro.au/research/pulsar/psrcat>

Table 4. Observing parameters and sensitivity thresholds for GC pulsar surveys conducted at 4–9 GHz

| Survey | ν_c (GHz) | B (GHz) | T (min.) | t_{samp} (ms) | $S_{\text{sys}}(\nu_c)^a$ (Jy) | $L_{\text{sh}}(\nu_c)^b$ (mJy kpc ²) | $L_{\text{min}}(\nu_c)^c$ (mJy kpc ²) | $L_{\text{min}}(6.1 \text{ GHz})^d$ (mJy kpc ²) |
|-----------------------------------|------------------|--------------|---------------|---------------------------|-----------------------------------|---|--|--|
| Johnston et al. (2006) | 8.4 | 0.864 | 70 | 1.0 | 148 | 22.1 | 3.5 | 5.5 |
| Deneva et al. (2009) | 4.8 | 0.8 | 60 | 0.65 | 57.5 ^e | 9.6 | 1.5 | 1.1 |
| Bates et al. (2011) | 6.59 | 0.576 | 280 | 0.13 | 216.7 | 19.8 | 3.2 | 3.5 |
| Eatough et al. (2021) | 4.85 | 0.5 | 72 | 0.26 | 129 | 24.9 | 4.0 | 2.9 |
| | 8.35 | 0.5 | 144 | 0.13 | 93.3 | 12.7 | 2.0 | 3.2 |
| This work ^f : | | | | | | | | |
| A00 | 6.1 | 3.35 | 30 | 0.35 | 46.3 | 5.3 | 0.9 | 0.9 |
| Off-Sgr A* pointings ^g | 6.1 | 3.35 | 5 | 0.35 | 10.7 | 3.0 | 0.5 | 0.5 |

$$^a S_{\text{sys}} = S_{\text{sys}}^{\text{off-GC}} + S_{\text{sys}}^{\text{SgrA*}}.$$

^bSingle harmonic pseudo-luminosity threshold, $L_{\text{sh}} = S_{\text{sh}} d_{\text{GC}}^2$, where $d_{\text{GC}} = 8.18$ kpc (Gravity Collaboration et al. 2019).

^cMinimum detectable pseudo-luminosity, $L_{\text{min}}(\nu_c) = S_{\text{min}}(\nu_c) d_{\text{GC}}^2$ for $\delta_{\text{int}} = 2.5\%$ and $P_0 = 1$ s.

^d $L_{\text{min}} \propto \nu^\alpha$ invoked, where $\alpha = -1.4$ is the mean pulsar spectral index (Bates et al. 2013).

^e $T_{\text{GC}}(\nu) \approx 568 \text{ K}(\nu/1 \text{ GHz})^{-1.13}$ (Rajwade et al. 2017) assumed to compute $S_{\text{sys}}^{\text{SgrA*}}$.

^fWe estimated $S_{\text{sys}}^{\text{off-GC}}$ and $S_{\text{sys}}^{\text{SgrA*}}$ using Figure 1 and Equation 2 of Suresh et al. (2021).

^gB-ring and C-ring pointings with negligible $S_{\text{sys}}^{\text{SgrA*}}$ in Figure 1.

Here, $\tau_{\text{sc}}(\nu)$ is the scatter-broadening time scale. In the absence of alternate observational evidence, we take τ_{sc} towards the GC magnetar to be representative of the central ISM throughout the remainder of our study. From Spitler et al. (2014), we have

$$\tau_{\text{sc}}(\nu) \simeq (1.3 \text{ s}) \nu_{c,\text{GHz}}^{-3.8}, \quad (10)$$

for GC magnetar pulses. Thus, scattering inhibits the detection of GC pulsars with $P_0 \leq \tau_{\text{sc}}(6.1 \text{ GHz}) \simeq 1.35$ ms.

Table 4 lists observational parameters and theoretical sensitivity limits of GC pulsar surveys conducted at ν_c between 4–9 GHz. We adopted a GC distance, $d_{\text{GC}} = 8.18$ kpc (Gravity Collaboration et al. 2019) to convert S_{sh} and S_{min} to pseudo-luminosities, L_{sh} and L_{min} , respectively. To facilitate sensitivity comparison

across surveys at different ν_c , we scaled their respective L_{min} to 6.1 GHz invoking $L_{\text{min}} \propto \nu^\alpha$, where $\alpha = -1.4$ is the mean pulsar spectral index (Bates et al. 2013). This scaling preserves the fraction of known pulsars with spectral pseudo-luminosity, $L_\nu \geq L_{\text{min}}(\nu)$ for a given survey.

Applying the above power-law scaling and assuming $\delta_{\text{int}} = 2.5\%$, Figure 7 shows $L_{\text{min}}(6.1 \text{ GHz})$ for various surveys as function of P_0 . Our survey clearly represents the most sensitive 4–8 GHz exploration for GC pulsars conducted to date. For $P_0 \gtrsim 100$ ms, our survey reaches down to $L_{\text{min}} \approx 0.9$ mJy kpc², i.e., a 18% improvement over Deneva et al. (2009), who also utilized the GBT for their observations. However, at $\nu_c = 4.8$ GHz, scattering limits the Deneva et al. (2009) sensitivity for

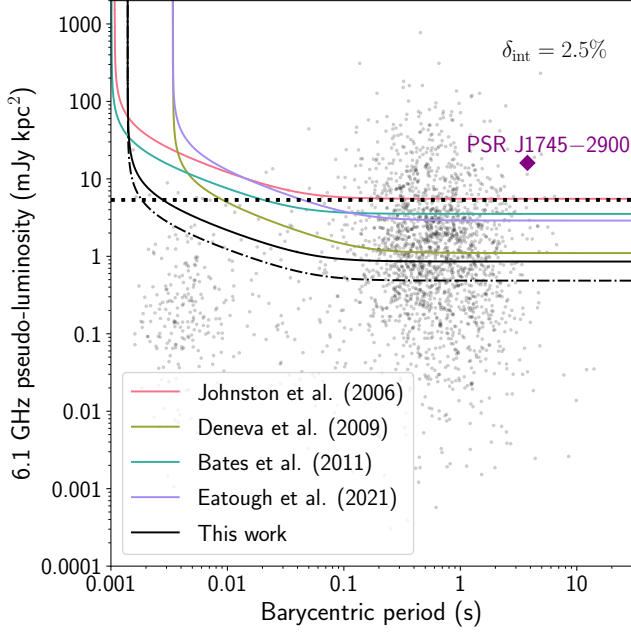


Figure 7. L_{\min} (6.1 GHz) curves for different GC pulsar surveys (various colors). The solid curves represent L_{\min} (6.1 GHz) for GC pointings at the survey parameters listed in Table 4. For [Eatough et al. \(2021\)](#), the plotted curve corresponds to their 4.85 GHz observations. The dash-dot black curves indicates L_{\min} for our $T = 5$ minutes pointings away from the Sgr A* complex. All curves assume $\delta_{\text{int}} = 2.5\%$ (median duty cycle for CPs). The black dotted line marks the single harmonic sensitivity for our $T = 30$ minutes GC scans. The background shows a scatter of 2197 pulsars with known 1.4 GHz flux densities ($S_{1.4}$) and known distances in the ATNF pulsar catalog v1.66. We scaled $S_{1.4}$ to 6.1 GHz assuming $S_\nu \propto \nu^\alpha$, where $\alpha = -1.4$ is the mean pulsar spectral index ([Bates et al. 2013](#)). The GC magnetar PSR J1745–2900 is highlighted with a purple diamond marker.

$P_0 \lesssim 100$ ms, with $P_0 \leq 3.4$ ms pulsars rendered undetectable. In contrast, our survey still provides significant sensitivity to $P_0 \geq 1.35$ ms, thereby extending our discovery phase space to include potential superluminous MSPs ($L_{6.1} \geq 6$ mJy kpc², $P_0 \approx 3$ ms) residing at the GC.

4.1. Fake Pulsar Injection and Recovery

Equations 6 and 8 describe our survey sensitivity presuming ideal Gaussian, white noise

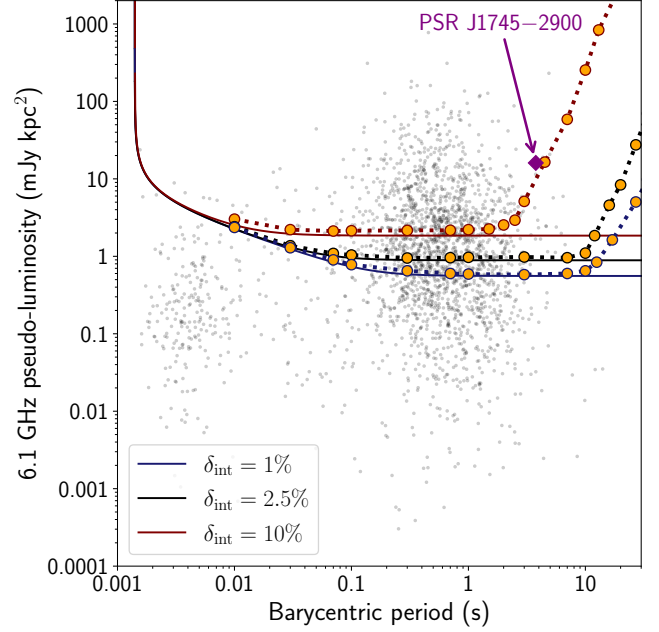


Figure 8. Theoretical (solid curves) and true sensitivity estimates (dotted curves) for different δ_{int} (various colors). All curves assume the survey parameters of our 30-minute A00 scans mentioned in Table 4. The duty cycles $\delta_{\text{int}} = 1\%$ (dark blue) and $\delta_{\text{int}} = 10\%$ (maroon) represent, respectively, the 10th and 93rd percentile of the empirical duty cycle distribution of CPs. The median δ_{int} of the corresponding distribution is 2.5% (black). The orange circular markers indicate minimum recovered 6.1 GHz pseudo-luminosities of fake pulsar injections at different trial δ_{int} and P_0 . As in Figure 7, the background plot is a scatter of 2197 pulsars from the ATNF pulsar catalog v1.66. The GC magnetar PSR J1745–2900 is labeled with a purple diamond marker.

backgrounds in dedispersed time series. However, real-world data frequently contains RFI and red noise, the latter of which substantially worsens our sensitivity to long P_0 ([Lazarus et al. 2015](#); [van Heerden et al. 2017](#)). Therefore, to measure our true survey sensitivity, we injected fake pulsars into our original dedispersed time series and verified their recovery.

Following Section 2.2 of [Suresh et al. \(2021\)](#), we first calibrated 11,016 dedispersed time se-

ries from six 30-minute A00 scans at epoch 4 (MJD 58738). To simulate a fake pulsar, we began with an input δ_{int} , P_0 , and a 6.1 GHz pseudo-luminosity $L_{6.1}$. We chose an initial pulse phase randomly from a standard uniform distribution. We then randomly drew Gaussian single pulse amplitudes \mathcal{A} and FWHMs W from lognormal distributions with means $(L_{6.1}/\delta_{\text{int}}d_{\text{GC}}^2)$ and $\delta_{\text{int}}P_0$ respectively. For both distributions, we assumed standard deviations equal to 5% of their respective means. To each W sample, we then added t_{samp} in quadrature. Utilizing the drawn \mathcal{A} and updated W samples, we thus generated a periodic Gaussian pulse train that models a discretely sampled signal at the location of a pulsar (pulse jitter neglected). We next incorporated scattering by convolving the simulated Gaussian pulse train with a one-sided, decaying exponential of time scale, $\tau_{\text{sc}}(6.1 \text{ GHz}) \simeq 1.35 \text{ ms}$. Finally, we added the resulting periodic signal to all calibrated time series to complete our fake pulsar injection. In the above exercise, we ignored instrumental and dispersive pulse broadening as these effects are negligible for the parameters of our survey and data processing (see Appendix B).

For every trial δ_{int} and P_0 , we kicked off our pulsar injections at $L_{6.1} = 0.8L_{\text{min}}$. Passing all calibrated time series containing the injected signal through our processing pipeline (including time series detrending), we stepped up $L_{6.1}$ in small increments until the detection significance of the artificial pulsar exceeded $6\sigma_{\text{ps}}$. Let $L_{\text{min}}^{\text{true}}$ denote the minimum recovered $L_{6.1}$ for a given trial δ_{int} and P_0 . Averaging $L_{\text{min}}^{\text{true}}$ over identical fake pulsar injections in 11,016 calibrated time series, we obtained the dotted sensitivity curves shown in Figure 8.

Noticeably, RFI raises our survey sensitivity above theoretical limits by 3–7% across all P_0 . Moreover, the presence of red noise in our raw

data progressively hinders our search sensitivity at longer P_0 and larger δ_{int} . However, despite the deleterious impact of red noise and RFI on our pulsar searches, our survey crucially retains adequate sensitivity to over 95% of theoretically detectable pulsars for a median CP δ_{int} of 2.5%.

5. SUMMARY AND DISCUSSION

We have conducted a comprehensive 4–8 GHz search of the central 6'25 ($\approx 14.9 \text{ pc}$ in projection) of our Galaxy for pulsars. Utilizing the GBT, our observing program comprised of 11 $T \geq 30$ minutes integrations on the GC and 53 $T = 5$ minutes integrations on nearby Galactic bulge fields. As proof of our survey integrity, we successfully demonstrated the detection of the GC magnetar PSR J1745–2900 in all of our GC scans. Executing Fourier-domain acceleration and jerk searches, we report the non-detection of hitherto unknown periodic astrophysical emissions in our data above a 6σ detection threshold.

Our investigations constitute the most sensitive 4–8 GHz exploration for GC pulsars conducted to date. For $\delta_{\text{int}} = 2.5\%$ and $P_0 \simeq 1 \text{ s}$, our survey reaches down to $L_{\text{min}}^{\text{true}} \approx 1 \text{ mJy kpc}^2$, i.e. a sensitivity improvement of at least 18% over past GC pulsar searches conducted at similar radio frequencies. Notably, our observations open the window to discovering potential superluminous MSPs ($L_{6.1} \geq 6 \text{ mJy kpc}^2$, $P_0 \approx 3 \text{ ms}$) at the GC. Though we focused our binary pulsar searches on CP orbits around Sgr A* or stellar-mass BHs, our chosen processing parameters in Table 2 also incorporate searches for bright MSPs with low radial pulsar accelerations ($z_{\text{max}} \lesssim 0.5P_{0,\text{ms}}^{-1}$) and jerks ($w_{\text{max}} \lesssim 1.1P_{0,\text{ms}}^{-1}$).

Studying pulsar demographics in our Galaxy, Freire (2013) argued that the globular cluster pulsar population is likely older than its Galactic field counterpart. Analogous to globular

clusters, the GC environment, with its high density of $\sim 10^6$ stars per cubic parsec (Schödel et al. 2018), is predicted to favor MSP production. About 3% of Galactic field MSPs have $L_{6.1} \geq L_{\min}^{\text{true}}$ of our survey. Say that GC MSPs follow similar population-level statistics as their Galactic field equivalents. For a beaming fraction $f_b = 0.7$ (Kramer et al. 1998), our non-detection of GC pulsars therefore constrains the total MSP count in the central parsec of our Galaxy to $N_{\text{MSP}} \lesssim 50$. Our N_{MSP} estimate is a factor of 20 smaller than that derived by Wharton et al. (2012) possibly due to our lack of sensitivity to tight MSP orbits. Sideband searches (Ransom et al. 2003) and coherent full-orbit demodulation algorithms (Allen et al. 2013; Balakrishnan et al. 2021) will both provide enhanced sensitivity to short binary orbital periods ($P_b \ll T$), thereby yielding stronger constraints on the GC MSP population in the near future.

Alternatively, our non-detection of GC pulsars can be attributed to complex pulsar orbital dynamics arising from plausible close encounters with other neutron stars, stellar-mass BHs, and intermediate-mass BHs in the dense GC environment. Such proximate compact object flybys can potentially disrupt binaries and scatter pulsars into hyperbolic orbits that lead away from the GC (Jiale Li et al. 2021). On the other hand, a preference for magnetar formation (Dexter & O’Leary 2014) at the GC may explain the “missing pulsar problem” by virtue of the comparatively shorter magnetar lifetimes ($\sim 10^4$ years).

Throughout our study, we presumed that interstellar scattering does not limit GC pulsar surveys. While $\tau_{\text{sc}}(\nu)$ measurements of the GC magnetar support the above premise, observa-

tions of pulse broadening along different lines of sight are necessary to build a more complete picture of the turbulent central ISM. Hence, we encourage regular monitoring of the GC for fast transients to obtain robust scattering constraints on the ionized central ISM, and thus better inform future GC pulsar surveys.

1 A.S. thanks Scott M. Ransom for timely re-
 2 sponses to software-related queries. A.S.,
 3 J.M.C., and S.C. acknowledge support from the
 4 National Science Foundation (AAG 1815242).
 5 J.M.C and S.C. are members of the NANOGrav
 6 Physics Frontiers Center, which is supported by
 7 the NSF award PHY-1430284. Breakthrough
 8 Listen is managed by the Breakthrough Ini-
 9 tiatives, sponsored by the Breakthrough Prize
 10 Foundation. The Green Bank Observatory is
 11 a facility of the National Science Foundation,
 12 operated under cooperative agreement by As-
 13 sociated Universities, Inc.

14
 15 This work used the Extreme Science
 16 and Engineering Discovery Environment
 17 (XSEDE) through allocations PHY200054
 18 and PHY210038, which is supported by
 19 National Science Foundation grant number
 20 ACI-1548562. Specifically, it used the Bridges-
 21 2 system, which is supported by NSF award
 22 number ACI-1928147, at the Pittsburgh Su-
 23 percomputing Center (PSC).

Facilities: GBT, XSEDE (Towns et al. 2014).

Software: Astropy (Astropy Collaboration et al. 2013, 2018), NumPy (van der Walt et al. 2011), Matplotlib (Hunter 2007), PRESTO (Ransom 2011), Python 3 (<https://www.python.org>), SciPy (Virtanen et al. 2020).

A. PULSE-AVERAGED PROFILES OF SAMPLE PERIODICITY CANDIDATES

Figures A1 and A2 show average profiles of two sample candidates that sit amidst the large scatter of detections between $P = 2$ ms and $P = 100$ ms in the P -DM plane of Figure 5. Average profiles were generated using the `prepfold` routine of PRESTO (Ransom 2011).

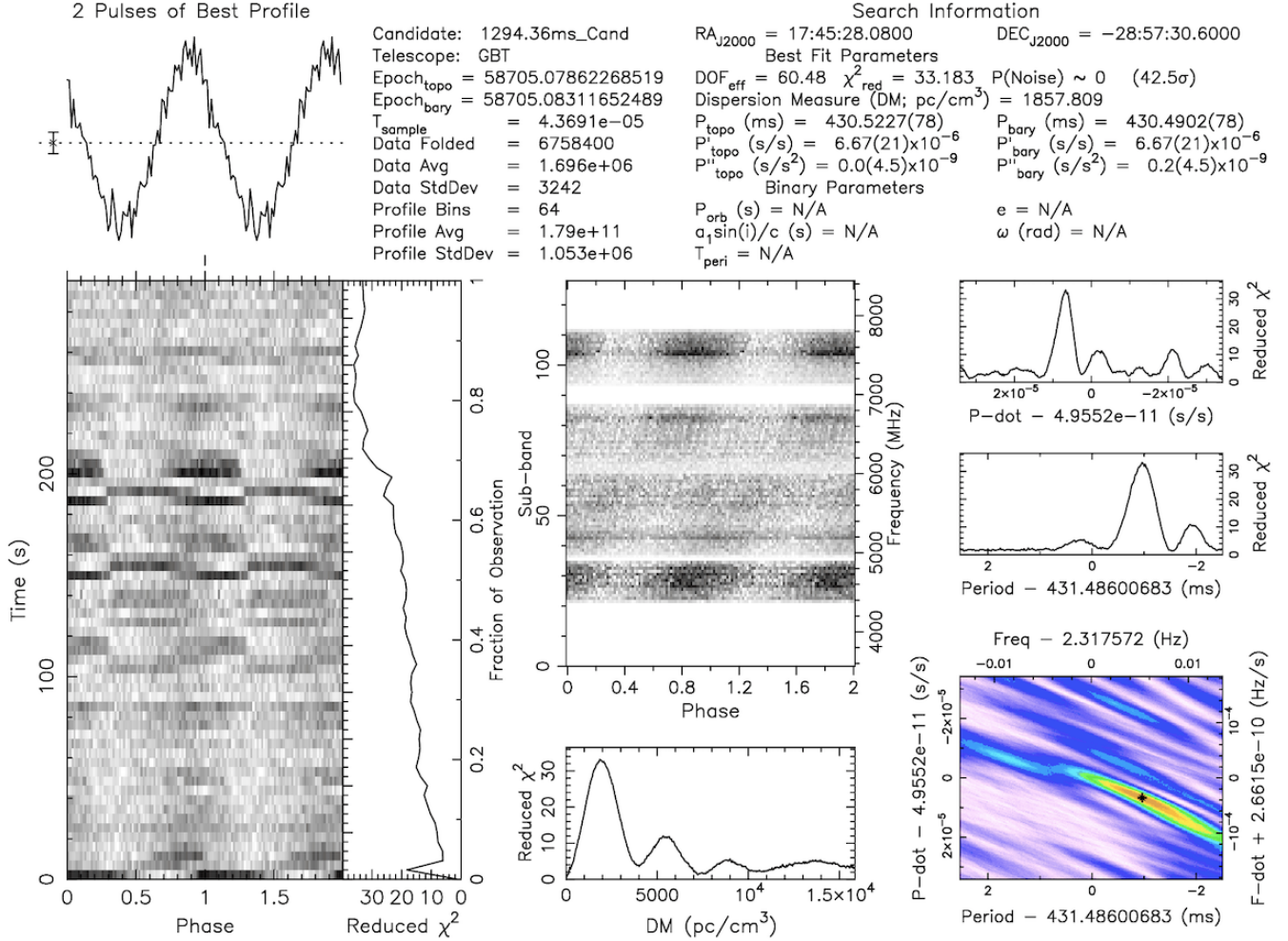


Figure A1. A sample periodicity detection in pointing C04 that falls within the sea of candidates between $P = 2$ ms and $P = 100$ ms in the P -DM plane (see Figure 5). Top left panel: Average pulse profile of candidate. Bottom left panel: Rotation-resolved profile with flux density shown on the grayscale. The reduced χ^2 measures the departure of the pulse-averaged profile from a flat noisy model. Top middle panel: Phase-resolved dynamic spectrum of candidate. Bottom middle panel: Variation of the reduced χ^2 with DM. Top right panel: Reduced χ^2 vs. period derivative (\dot{P}). Central right panel: Reduced χ^2 vs. folding period (P). Bottom right panel: Raster plot of the reduced χ^2 in the P - \dot{P} plane. The pulsation significance (42.5 σ) quoted in the top right corner quantifies the equivalent Gaussian detection probability determined from the reduced χ^2 of the average profile.

B. EFFECTIVE SINGLE PULSE WIDTHS IN DEDISPERSED TIME SERIES

Consider a pulsar emitting single pulses of average intrinsic width W_{int} . Accounting for instrumental effects, sampling, and propagation-induced broadening, the effective pulse width in a dedispersed time

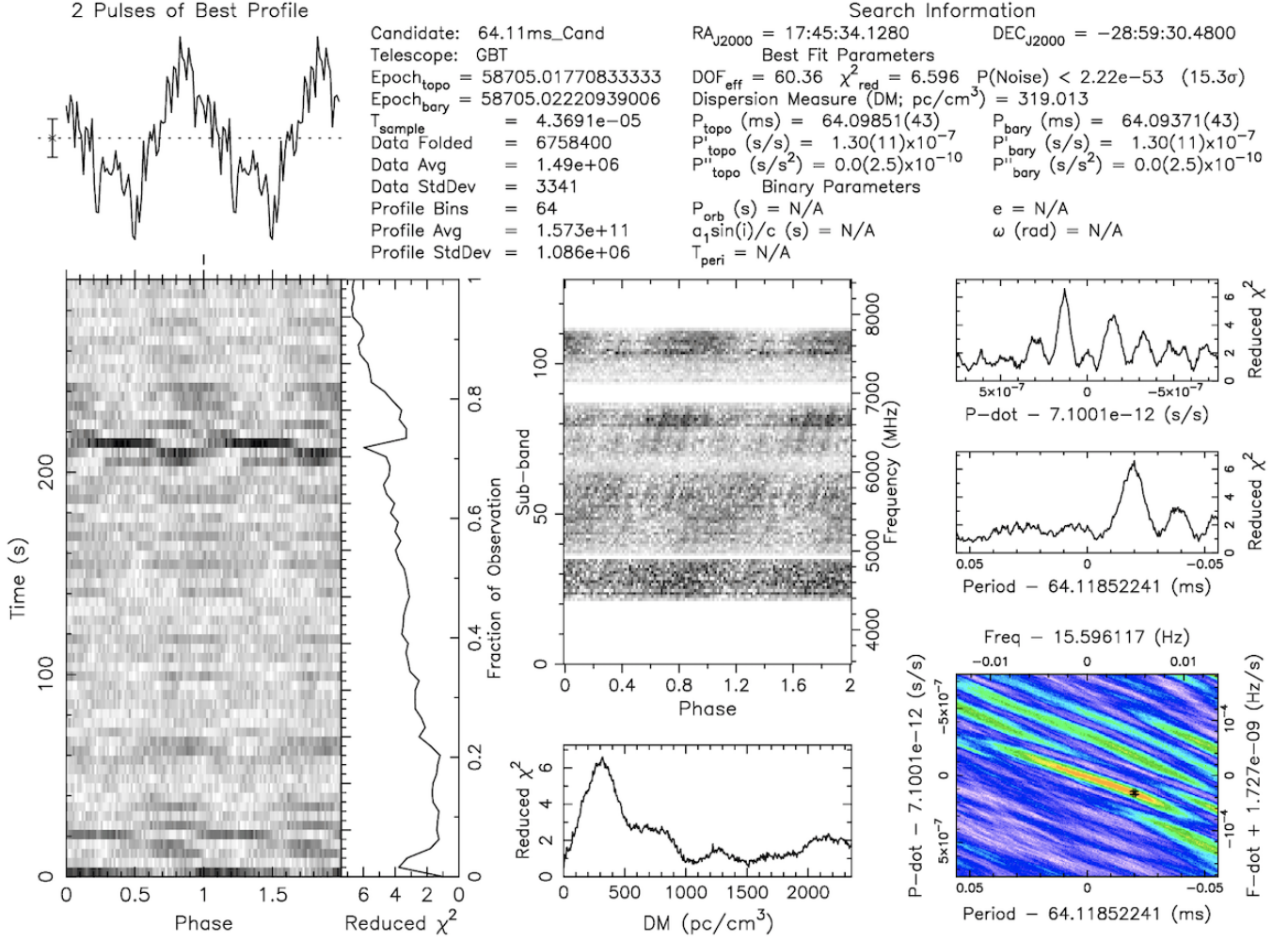


Figure A2. A prepfold output of a periodicity detection in pointing B02.

series is

$$W_{\text{eff}} = (W_{\text{int}}^2 + t_{\text{samp}}^2 + t_R^2 + t_{\text{chan}}^2 + t_{\text{BW}}^2 + \tau_{\text{sc}}^2)^{1/2}. \quad (\text{B1})$$

Here, t_{samp} is the sample interval in the dedispersed time series, and $t_R \sim (\Delta\nu_{\text{ch}})^{-1}$ is the receiver filter response time for a channel bandwidth $\Delta\nu_{\text{ch}}$.

The term t_{chan} represents the intrachannel dispersive smearing given by (Cordes & McLaughlin 2003)

$$t_{\text{chan}} \approx 8.3 \mu\text{s} \left(\frac{\text{DM}_{\text{pc cm}^{-3}} \Delta\nu_{\text{ch, MHz}}}{\nu_{c, \text{GHz}}^3} \right). \quad (\text{B2})$$

Further, t_{BW} quantifies the residual broadband dispersive delay for a DM error δDM .

$$t_{\text{BW}} \approx 8.3 \mu\text{s} \left(\frac{\delta\text{DM}_{\text{pc cm}^{-3}} B_{\text{MHz}}}{\nu_{c, \text{GHz}}^3} \right). \quad (\text{B3})$$

Finally, $\tau_{\text{sc}}(\nu)$ is the pulse-broadening time scale from multi-path wave propagation through turbulent ionized plasma.

For our observations, $\nu_c \approx 6.1$ GHz, $B \approx 3.35$ GHz, $\Delta\nu_{\text{ch}} \approx 91.67$ kHz, and $t_{\text{samp}} \approx 349.53 \mu\text{s}$. Working with a DM step size of 3 pc cm^{-3} , our trial DMs are at best, $\delta\text{DM} = 1.5 \text{ pc cm}^{-3}$ off from the true DM of a source. Collectively, the above numbers imply $t_R \sim 11 \mu\text{s}$, $t_{\text{BW}} \approx 184 \mu\text{s}$, and $t_{\text{chan}} \approx 6 \mu\text{s}$ for $\text{DM} = 1776 \text{ pc cm}^{-3}$ of the GC magnetar (Suresh et al. 2021). Assuming the empirical GC magnetar scattering law (Spitler et al. 2014) given in Equation 10, $\tau_{\text{sc}} \simeq 1.35$ ms at 6.1 GHz.

Since $\tau_{\text{sc}} \gg t_{\text{chan}}, t_{\text{BW}}, t_R$, Equation B1 can thus be simplified to

$$W_{\text{eff}}(\nu) = (W_{\text{int}}^2 + t_{\text{samp}}^2 + \tau_{\text{sc}}^2(\nu))^{1/2}. \quad (\text{B4})$$

REFERENCES

- Abazajian, K. N., Canac, N., Horiuchi, S., & Kaplinghat, M. 2014, *PhRvD*, 90, 023526, doi: [10.1103/PhysRevD.90.023526](https://doi.org/10.1103/PhysRevD.90.023526)
- Ackermann, M., Albert, A., Atwood, W. B., et al. 2014, *ApJ*, 793, 64, doi: [10.1088/0004-637X/793/1/64](https://doi.org/10.1088/0004-637X/793/1/64)
- Ajello, M., Albert, A., Atwood, W. B., et al. 2016, *ApJ*, 819, 44, doi: [10.3847/0004-637X/819/1/44](https://doi.org/10.3847/0004-637X/819/1/44)
- Allen, B., Knispel, B., Cordes, J. M., et al. 2013, *ApJ*, 773, 91, doi: [10.1088/0004-637X/773/2/91](https://doi.org/10.1088/0004-637X/773/2/91)
- Andersen, B. C., & Ransom, S. M. 2018, *ApJL*, 863, L13, doi: [10.3847/2041-8213/aad59f](https://doi.org/10.3847/2041-8213/aad59f)
- Astropy Collaboration, Robitaille, T. P., Tollerud, E. J., et al. 2013, *A&A*, 558, A33, doi: [10.1051/0004-6361/201322068](https://doi.org/10.1051/0004-6361/201322068)
- Astropy Collaboration, Price-Whelan, A. M., Sipócz, B. M., et al. 2018, *AJ*, 156, 123, doi: [10.3847/1538-3881/aabc4f](https://doi.org/10.3847/1538-3881/aabc4f)
- Bagchi, M., Lorimer, D. R., & Wolfe, S. 2013, *MNRAS*, 432, 1303, doi: [10.1093/mnras/stt559](https://doi.org/10.1093/mnras/stt559)
- Balakrishnan, V., Champion, D., Barr, E., et al. 2021, *MNRAS*, doi: [10.1093/mnras/stab3746](https://doi.org/10.1093/mnras/stab3746)
- Bartels, R., Krishnamurthy, S., & Weniger, C. 2016, *PhRvL*, 116, 051102, doi: [10.1103/PhysRevLett.116.051102](https://doi.org/10.1103/PhysRevLett.116.051102)
- Bates, S. D., Lorimer, D. R., & Verbiest, J. P. W. 2013, *MNRAS*, 431, 1352, doi: [10.1093/mnras/stt257](https://doi.org/10.1093/mnras/stt257)
- Bates, S. D., Johnston, S., Lorimer, D. R., et al. 2011, *MNRAS*, 411, 1575, doi: [10.1111/j.1365-2966.2010.17790.x](https://doi.org/10.1111/j.1365-2966.2010.17790.x)
- Brandt, T. D., & Kocsis, B. 2015, *ApJ*, 812, 15, doi: [10.1088/0004-637X/812/1/15](https://doi.org/10.1088/0004-637X/812/1/15)
- Calore, F., Cholis, I., McCabe, C., & Weniger, C. 2015, *PhRvD*, 91, 063003, doi: [10.1103/PhysRevD.91.063003](https://doi.org/10.1103/PhysRevD.91.063003)
- Chiti, A., Chatterjee, S., Wharton, R., et al. 2016, *ApJ*, 833, 11, doi: [10.3847/0004-637X/833/1/11](https://doi.org/10.3847/0004-637X/833/1/11)
- Cordes, J. M., & Lazio, T. J. W. 1997, *ApJ*, 475, 557, doi: [10.1086/303569](https://doi.org/10.1086/303569)
- Cordes, J. M., & Lazio, T. J. W. 2002, arXiv e-prints, astro, <https://arxiv.org/abs/astro-ph/0207156>
- Cordes, J. M., & McLaughlin, M. A. 2003, *ApJ*, 596, 1142, doi: [10.1086/378231](https://doi.org/10.1086/378231)
- Cromartie, H. T., Fonseca, E., Ransom, S. M., et al. 2020, *Nature Astronomy*, 4, 72, doi: [10.1038/s41550-019-0880-2](https://doi.org/10.1038/s41550-019-0880-2)
- Deneva, J. S., Cordes, J. M., & Lazio, T. J. W. 2009, *ApJL*, 702, L177, doi: [10.1088/0004-637X/702/2/L177](https://doi.org/10.1088/0004-637X/702/2/L177)
- Dewey, R. J., Taylor, J. H., Weisberg, J. M., & Stokes, G. H. 1985, *ApJL*, 294, L25, doi: [10.1086/184502](https://doi.org/10.1086/184502)
- Dexter, J., & O’Leary, R. M. 2014, *ApJL*, 783, L7, doi: [10.1088/2041-8205/783/1/L7](https://doi.org/10.1088/2041-8205/783/1/L7)
- Dexter, J., Deller, A., Bower, G. C., et al. 2017, *MNRAS*, 471, 3563, doi: [10.1093/mnras/stx1777](https://doi.org/10.1093/mnras/stx1777)

- Eatough, R. P., Kramer, M., Klein, B., et al. 2013a, in *Neutron Stars and Pulsars: Challenges and Opportunities after 80 years*, ed. J. van Leeuwen, Vol. 291, 382–384, doi: [10.1017/S1743921312024209](https://doi.org/10.1017/S1743921312024209)
- Eatough, R. P., Falcke, H., Karuppusamy, R., et al. 2013b, *Nature*, 501, 391, doi: [10.1038/nature12499](https://doi.org/10.1038/nature12499)
- Eatough, R. P., Torne, P., Desvignes, G., et al. 2021, *MNRAS*, 507, 5053, doi: [10.1093/mnras/stab2344](https://doi.org/10.1093/mnras/stab2344)
- Fragione, G., Antonini, F., & Gnedin, O. Y. 2018, *MNRAS*, 475, 5313, doi: [10.1093/mnras/sty183](https://doi.org/10.1093/mnras/sty183)
- Freire, P. C. C. 2013, in *Neutron Stars and Pulsars: Challenges and Opportunities after 80 years*, ed. J. van Leeuwen, Vol. 291, 243–250, doi: [10.1017/S1743921312023770](https://doi.org/10.1017/S1743921312023770)
- Gajjar, V., Perez, K. I., Siemion, A. P. V., et al. 2021, *AJ*, 162, 33, doi: [10.3847/1538-3881/abfd36](https://doi.org/10.3847/1538-3881/abfd36)
- Genzel, R., Eisenhauer, F., & Gillessen, S. 2010, *Reviews of Modern Physics*, 82, 3121, doi: [10.1103/RevModPhys.82.3121](https://doi.org/10.1103/RevModPhys.82.3121)
- Ghez, A. M., Salim, S., Hornstein, S. D., et al. 2005, *ApJ*, 620, 744, doi: [10.1086/427175](https://doi.org/10.1086/427175)
- Gravity Collaboration, Abuter, R., Amorim, A., et al. 2019, *A&A*, 625, L10, doi: [10.1051/0004-6361/201935656](https://doi.org/10.1051/0004-6361/201935656)
- GRAVITY Collaboration, Abuter, R., Aymar, N., et al. 2021, arXiv e-prints, arXiv:2112.07478. <https://arxiv.org/abs/2112.07478>
- Hailey, C. J., Mori, K., Bauer, F. E., et al. 2018, *Nature*, 556, 70, doi: [10.1038/nature25029](https://doi.org/10.1038/nature25029)
- Hunter, J. D. 2007, *Computing in Science Engineering*, 9, 90, doi: [10.1109/MCSE.2007.55](https://doi.org/10.1109/MCSE.2007.55)
- Hyman, S. D., Lazio, T. J. W., Kassim, N. E., et al. 2005, *Nature*, 434, 50, doi: [10.1038/nature03400](https://doi.org/10.1038/nature03400)
- Hyman, S. D., Wijnands, R., Lazio, T. J. W., et al. 2009, *ApJ*, 696, 280, doi: [10.1088/0004-637X/696/1/280](https://doi.org/10.1088/0004-637X/696/1/280)
- Hyman, S. D., Frail, D. A., Deneva, J. S., et al. 2021, *MNRAS*, 507, 3888, doi: [10.1093/mnras/stab1979](https://doi.org/10.1093/mnras/stab1979)
- Jiale Li, K., Wu, K., Leung, P. K., & Singh, D. 2021, arXiv e-prints, arXiv:2110.03494. <https://arxiv.org/abs/2110.03494>
- Johnston, S., Kramer, M., Lorimer, D. R., et al. 2006, *MNRAS*, 373, L6, doi: [10.1111/j.1745-3933.2006.00232.x](https://doi.org/10.1111/j.1745-3933.2006.00232.x)
- Kramer, M., Backer, D. C., Cordes, J. M., et al. 2004, *NewAR*, 48, 993, doi: [10.1016/j.newar.2004.09.020](https://doi.org/10.1016/j.newar.2004.09.020)
- Kramer, M., Xilouris, K. M., Lorimer, D. R., et al. 1998, *ApJ*, 501, 270, doi: [10.1086/305790](https://doi.org/10.1086/305790)
- Law, C. J., Yusef-Zadeh, F., Cotton, W. D., & Maddalena, R. J. 2008, *ApJS*, 177, 255, doi: [10.1086/533587](https://doi.org/10.1086/533587)
- Lazarus, P., Brazier, A., Hessels, J. W. T., et al. 2015, *ApJ*, 812, 81, doi: [10.1088/0004-637X/812/1/81](https://doi.org/10.1088/0004-637X/812/1/81)
- Lazio, T. J. W., & Cordes, J. M. 1998a, *ApJS*, 118, 201, doi: [10.1086/313129](https://doi.org/10.1086/313129)
- . 1998b, *ApJ*, 505, 715, doi: [10.1086/306174](https://doi.org/10.1086/306174)
- Lebofsky, M., Croft, S., Siemion, A. P. V., et al. 2019, *PASP*, 131, 124505, doi: [10.1088/1538-3873/ab3e82](https://doi.org/10.1088/1538-3873/ab3e82)
- Lee, S. K., Lisanti, M., & Safdi, B. R. 2015, *JCAP*, 2015, 056, doi: [10.1088/1475-7516/2015/05/056](https://doi.org/10.1088/1475-7516/2015/05/056)
- Liu, K., Wex, N., Kramer, M., Cordes, J. M., & Lazio, T. J. W. 2012, *ApJ*, 747, 1, doi: [10.1088/0004-637X/747/1/1](https://doi.org/10.1088/0004-637X/747/1/1)
- Liu, K., Desvignes, G., Eatough, R. P., et al. 2021, *ApJ*, 914, 30, doi: [10.3847/1538-4357/abf9a2](https://doi.org/10.3847/1538-4357/abf9a2)
- MacMahon, D. H. E., Price, D. C., Lebofsky, M., et al. 2018, *PASP*, 130, 044502, doi: [10.1088/1538-3873/aa80d2](https://doi.org/10.1088/1538-3873/aa80d2)
- Macquart, J. P., Kanekar, N., Frail, D. A., & Ransom, S. M. 2010, *ApJ*, 715, 939, doi: [10.1088/0004-637X/715/2/939](https://doi.org/10.1088/0004-637X/715/2/939)
- Manchester, R. N., Lyne, A. G., Camilo, F., et al. 2001, *MNRAS*, 328, 17, doi: [10.1046/j.1365-8711.2001.04751.x](https://doi.org/10.1046/j.1365-8711.2001.04751.x)
- Paumard, T., Maillard, J. P., Morris, M., & Rigaut, F. 2001, *A&A*, 366, 466, doi: [10.1051/0004-6361:20000227](https://doi.org/10.1051/0004-6361:20000227)
- Penrose, R. 1969, *Nuovo Cimento Rivista Serie*, 1, 252
- . 1999, *Journal of Astrophysics and Astronomy*, 20, 233, doi: [10.1007/BF02702355](https://doi.org/10.1007/BF02702355)
- Psaltis, D., Wex, N., & Kramer, M. 2016, *ApJ*, 818, 121, doi: [10.3847/0004-637X/818/2/121](https://doi.org/10.3847/0004-637X/818/2/121)
- Rajwade, K. M., Lorimer, D. R., & Anderson, L. D. 2017, *MNRAS*, 471, 730, doi: [10.1093/mnras/stx1661](https://doi.org/10.1093/mnras/stx1661)
- Ransom, S. 2011, *PRESTO: Pulsar Exploration and Search TOolkit*. <http://ascl.net/1107.017>

- Ransom, S. M. 2008, in *Dynamical Evolution of Dense Stellar Systems*, ed. E. Vesperini, M. Giersz, & A. Sills, Vol. 246, 291–300, doi: [10.1017/S1743921308015810](https://doi.org/10.1017/S1743921308015810)
- Ransom, S. M., Cordes, J. M., & Eikenberry, S. S. 2003, *ApJ*, 589, 911, doi: [10.1086/374806](https://doi.org/10.1086/374806)
- Ransom, S. M., Eikenberry, S. S., & Middleditch, J. 2002, *AJ*, 124, 1788, doi: [10.1086/342285](https://doi.org/10.1086/342285)
- Schnitzeler, D. H. F. M., Eatough, R. P., Ferrière, K., et al. 2016, *MNRAS*, 459, 3005, doi: [10.1093/mnras/stw841](https://doi.org/10.1093/mnras/stw841)
- Schödel, R., Gallego-Cano, E., Dong, H., et al. 2018, *A&A*, 609, A27, doi: [10.1051/0004-6361/201730452](https://doi.org/10.1051/0004-6361/201730452)
- Schödel, R., Noguerras-Lara, F., Gallego-Cano, E., et al. 2020, *A&A*, 641, A102, doi: [10.1051/0004-6361/201936688](https://doi.org/10.1051/0004-6361/201936688)
- Schödel, R., Eckart, A., Alexander, T., et al. 2007, *A&A*, 469, 125, doi: [10.1051/0004-6361:20065089](https://doi.org/10.1051/0004-6361:20065089)
- Siemion, A., Bailes, M., Bower, G., et al. 2013, in *Neutron Stars and Pulsars: Challenges and Opportunities after 80 years*, ed. J. van Leeuwen, Vol. 291, 57–57, doi: [10.1017/S1743921312023149](https://doi.org/10.1017/S1743921312023149)
- Spitler, L. G., Lee, K. J., Eatough, R. P., et al. 2014, *ApJL*, 780, L3, doi: [10.1088/2041-8205/780/1/L3](https://doi.org/10.1088/2041-8205/780/1/L3)
- Suresh, A., Cordes, J. M., Chatterjee, S., et al. 2021, *ApJ*, 921, 101, doi: [10.3847/1538-4357/ac1d45](https://doi.org/10.3847/1538-4357/ac1d45)
- Torne, P., Desvignes, G., Eatough, R. P., et al. 2021, *A&A*, 650, A95, doi: [10.1051/0004-6361/202140775](https://doi.org/10.1051/0004-6361/202140775)
- Towns, J., Cockerill, T., Dahan, M., et al. 2014, *Computing in Science and Engineering*, 16, 62, doi: [10.1109/MCSE.2014.80](https://doi.org/10.1109/MCSE.2014.80)
- van der Walt, S., Colbert, S. C., & Varoquaux, G. 2011, *Computing in Science Engineering*, 13, 22, doi: [10.1109/MCSE.2011.37](https://doi.org/10.1109/MCSE.2011.37)
- van Heerden, E., Karastergiou, A., & Roberts, S. J. 2017, *MNRAS*, 467, 1661, doi: [10.1093/mnras/stw3068](https://doi.org/10.1093/mnras/stw3068)
- Virtanen, P., Gommers, R., Oliphant, T. E., et al. 2020, *Nature Methods*, 17, 261, doi: [10.1038/s41592-019-0686-2](https://doi.org/10.1038/s41592-019-0686-2)
- Wex, N. 2014, arXiv e-prints, arXiv:1402.5594. <https://arxiv.org/abs/1402.5594>
- Wex, N., & Kopeikin, S. M. 1999, *ApJ*, 514, 388, doi: [10.1086/306933](https://doi.org/10.1086/306933)
- Wharton, R. S., Chatterjee, S., Cordes, J. M., Deneva, J. S., & Lazio, T. J. W. 2012, *ApJ*, 753, 108, doi: [10.1088/0004-637X/753/2/108](https://doi.org/10.1088/0004-637X/753/2/108)
- Wosley, S. E., Sukhbold, T., & Janka, H. T. 2020, *ApJ*, 896, 56, doi: [10.3847/1538-4357/ab8cc1](https://doi.org/10.3847/1538-4357/ab8cc1)
- Zhang, C. M., Wang, J., Zhao, Y. H., et al. 2011, *A&A*, 527, A83, doi: [10.1051/0004-6361/201015532](https://doi.org/10.1051/0004-6361/201015532)
- Zhao, J.-H., Morris, M. R., & Goss, W. M. 2016, *ApJ*, 817, 171, doi: [10.3847/0004-637X/817/2/171](https://doi.org/10.3847/0004-637X/817/2/171)
- . 2020, *ApJ*, 905, 173, doi: [10.3847/1538-4357/abc75e](https://doi.org/10.3847/1538-4357/abc75e)
- . 2022, arXiv e-prints, arXiv:2202.05300. <https://arxiv.org/abs/2202.05300>
- Zhu, Z., Li, Z., & Morris, M. R. 2018, *ApJS*, 235, 26, doi: [10.3847/1538-4365/aab14f](https://doi.org/10.3847/1538-4365/aab14f)